

Characterization of a 64 Channel PET Detector Using Photodiodes for Crystal Identification*

J. S. Huber[†], *Member, IEEE*, W.W. Moses[†], *Senior Member, IEEE*, S.E. Derenzo[†], *Senior Member, IEEE*, M.H. Ho[†], M.S. Andreaco[‡], M.J. Paulus[‡], *Member, IEEE*, and R. Nutt[‡], *Fellow, IEEE*

[†]Lawrence Berkeley National Laboratory, University of California, Berkeley, CA 94720

[‡]CTI, Inc., Knoxville, TN 37932

Abstract

We present performance results for a prototype PET detector module consisting of 64 LSO scintillator crystals (3x3x20 mm) coupled on one end to a single photomultiplier tube and on the opposite end to a 64 pixel array of 3 mm square silicon photodiodes (typical pixel parameters are 5 pF capacitance, 300 pA dark current, and 73% quantum efficiency at 415 nm). The photomultiplier tube (PMT) provides an accurate timing pulse and energy threshold for all crystals in the module, the silicon photodiodes (PD) identify the crystal of interaction, the sum (PD+PMT) provides a total energy signal, and the PD/(PD+PMT) ratio determines the depth of interaction. With 32 of the channels instrumented, the detector module correctly identifies the crystal of interaction (where “correct” includes the adjacent 4 crystals) $79\pm 4\%$ of the time with high detection efficiency. The timing resolution for a single LSO detector module is 750 ps fwhm, while its pulse height resolution at 511 keV is $24\pm 3\%$ fwhm. The depth of interaction (DOI) measurement resolution is 8 ± 1 mm fwhm.

I. INTRODUCTION

A high resolution PET detector requires both the use of narrow crystals and the measurement of the annihilation photon’s depth of interaction within a crystal. We have previously presented design studies and prototype results for several high rate, high resolution PET detector modules that utilize a single photomultiplier tube to provide an accurate timing pulse and initial energy discrimination for a group of 3 mm square by 25–30 mm deep scintillator crystals, in combination with a silicon photodiode array to identify the crystal of interaction and possibly the depth of interaction (figure 1). These studies have shown encouraging room temperature results with both BGO scintillator (which is only capable of identifying the crystal of interaction) [1] and LSO scintillator (which is also capable of measuring depth of interaction) [2]. However, the prototype detector modules used to obtain these results had a maximum of four scintillator crystal/photodiode elements due to the lack of a suitable 64 element photodiode array. This raises questions about whether the technologies employed can be scaled up to a full 64

element detector module and still yield a practical design. In this paper we report results of measurements made on a 64 element detector module made with LSO scintillator crystal.

We prefer this ratio based technique to determine the depth of interaction because: (a) it is less sensitive to patient Compton scatter than approaches that use a single photodetector [3]; (b) it obtains better DOI resolution than approaches that use physically segmented crystals [4–6]; and (c) it has a smaller deadtime-surface area product than approaches that use large scintillator plates [7].

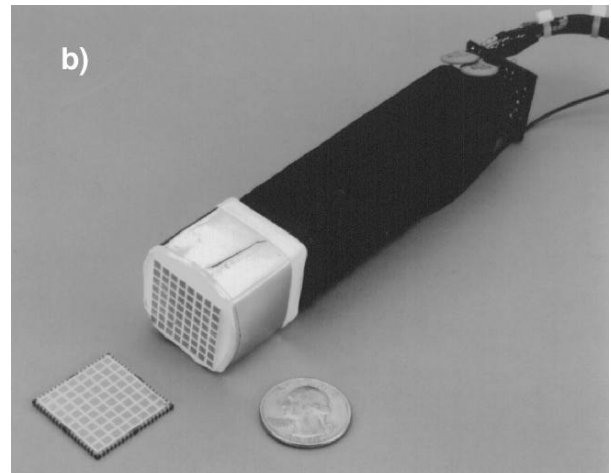
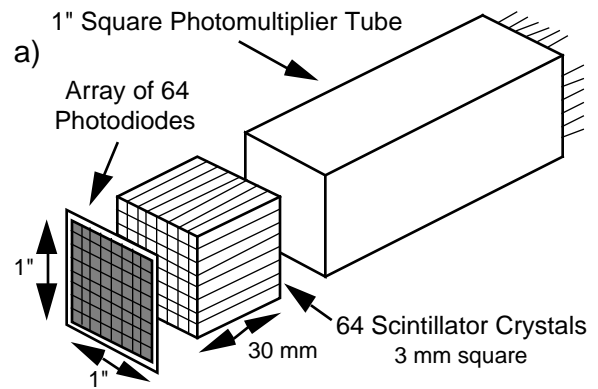


Figure 1: a) Diagram of the PET module. Each crystal is attached to a photomultiplier tube, which provides timing and initial energy information, and to a photodiode, which identifies the crystal of interaction. The PMT and PD signals are combined to measure the depth of interaction and total energy. b) Photograph of the 64 channel LSO detector module. The PMT, crystal array, and photodiode array are shown prior to attaching the photodiode array.

* This work was supported in part by the U.S. Department of Energy under Contract No. DE-AC03-76SF00098, in part by Public Health Service Grant Nos. P01-HL25840, R01-CA67911, and R01-NS29655, and in part by Breast Cancer Research Program of the University of California Grant No. 1RB-0068.

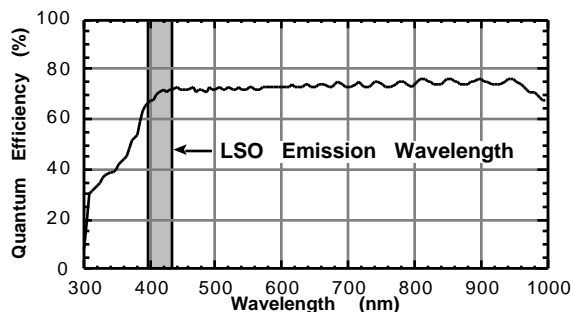


Figure 2: Quantum efficiency vs. wavelength for the photodiode array, showing 73% quantum efficiency for the 415 nm emissions of LSO.

II. INDIVIDUAL COMPONENTS

A. Scintillator Crystal Array

The detector module is constructed by coupling a 64 element LSO crystal array onto a 1 inch square Hamamatsu R-2497 photomultiplier tube. The 2.7x2.7x20 mm LSO scintillator crystals are arranged into an 8x8 array on a 3 mm pitch. Compromises were made due to the limited availability of LSO scintillator material (grown by Schlumberger-Doll Research, Ridgefield, CT) [8]. The length of the crystal is 20 mm because of insufficient starting material long enough to make 30 mm crystals. In addition, individual crystals come from a number of separate growth runs and have lower than “typical” LSO light output. When the crystals are polished and wrapped with Teflon reflector material, the mean light output is approximately 12,000 photons/MeV. This is measured by comparing 511 keV photopeak positions with a NaI(Tl) crystal assumed to have 38,000 photons/MeV output. This light output is higher than BGO but one third of the “best” LSO. These crystals are then etched and individually wrapped with Teflon to provide a depth dependent light collection ratio while preserving the total light collection efficiency.

B. Photodiode Array

Each pixel of the 64 element, 3 mm pitch photodiode array (provided by Hamamatsu Photonics) is 2.8 mm square, except for those elements on the periphery. Because electrical connections to the photodiode elements are made on a 1.2 mm wide optically inactive region around the perimeter of the diode array, the size of the corner elements is reduced to 2.5 mm square and the remainder of the elements on the periphery are reduced to 2.5x2.8 mm. This degrades the optical coupling to the crystal elements on the edge of the detector array, but allows the inactive region (*i.e.* insensitive to 511 keV gamma rays) between two adjacent detector modules to be reduced.

The silicon PIN photodiode array has a 300 μm depletion thickness and each element has a 3–6 pF capacitance (measured at the perimeter of the array), with elements toward the center having higher capacitance due to the longer lead length. With a 50 V bias, the dark current at 25° C is 200–400 pA per element with no systematic dependence on

location. The quantum efficiency, shown in figure 2, is approximately 73% for the 415 nm emissions of LSO.

C. Electronics

Amplification for the photodiodes is provided by 2 mm square ICs containing 16 low noise charge sensitive preamplifiers and shaper amplifiers [9]. The noise when coupled to the photodiode is $\sim 220 e^-$ rms at an amplifier peaking time of 1.4 μsec , which is used for all measurements.

An amplifier IC is read out with a custom CAMAC module that amplifies and simultaneously samples the 16 output voltages, then passes the 16 held analog voltages to a scanning ADC for digitization and computer readout. Two such boards are used, allowing readout of 32 channels. Calibration and channel dependent corrections are then applied in software, as is the identification of the channel with the largest voltage. The scanning ADC limits this configuration to a relatively low rate capability (~ 1 khz).

An alternative method for rapidly (< 50 ns) identifying the crystal of interaction is a “Winner-Take-All” (WTA) circuit. Given n analog input voltages, the WTA circuit rapidly determines which input has the highest voltage and outputs the encoded address of this channel [10]. A 16 input integrated circuit of this type includes a common strobe sample and hold on each input (so that the channels can be simultaneously compared) and a buffered analog output that is proportional to the voltage of the “winner” (*i.e.* the channel with the highest voltage). Unfortunately the WTA circuit is not used in these measurements due to crystal to crystal light output variations in the LSO array that require channel to channel gain compensation, which is not possible in the present amplifier IC.

III. DETECTOR PERFORMANCE

A. General Characterization

The detector module is excited with a beam of 511 keV photons that is electronically collimated (3.1 mm fwhm) using a single 3x3x30 mm BGO crystal coupled to a photomultiplier tube, and aligned with the photodiode end of a “target” crystal in the detector module (figure 3). Whenever the photomultiplier tube detects an energy deposit greater than 150 keV (in time coincidence with the collimating photomultiplier tube), signals from the 32 instrumented elements are read out. The photodiode and photomultiplier tube signals are calibrated and converted into an equal energy scale using the

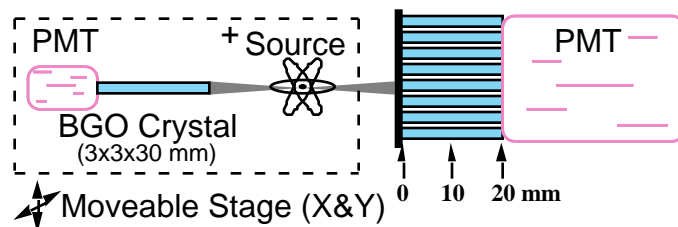


Figure 3: Experimental set-up. The + source, 3x3x30 mm BGO crystal, and PMT provide an electronically collimated beam (3.1 mm fwhm) whose position is adjusted by moving the stage.

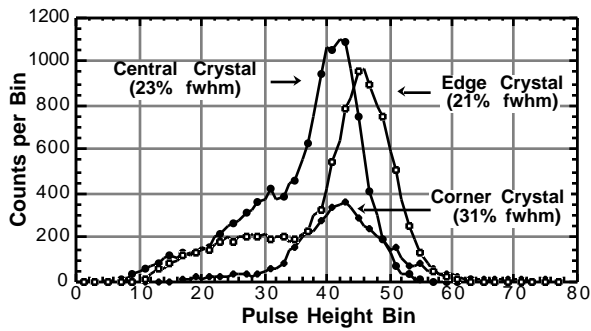


Figure 4: 511 keV pulse height spectra of a central, edge and corner LSO crystal, as observed by the photodiode summed with the common photomultiplier tube (PD+PMT) signal.

method described in the next section. The channel with the greatest photodiode pulse height is then defined to be the crystal of interaction; this photodiode signal is added to the photomultiplier tube signal to provide a depth independent “total energy” signal for characterization measurements. A total energy threshold of 300 keV is applied to the summed signals.

Using this total energy signal, the pulse height resolution of the detector is $24 \pm 3\%$ fwhm based on the fourteen channels measured. The crystal in the corner position is the only channel found to be significantly different with a resolution of 31% fwhm. Figure 4 shows the 511 keV pulse height distribution for three individual crystals.

Figure 5 shows several end-on views of the 8 by 8 array of square scintillator crystals, each with a different “target” crystal (identified by a heavy border). The numbers in each square represent the percentage of photomultiplier tube triggers in which the interaction is assigned to that crystal. As figure 5 demonstrates, the correct crystal of interaction is assigned $55 \pm 6\%$ of the time (based on measurements of all instrumented channels) when a total energy threshold of 300 keV is used. This compares favorably with conventional block detectors, which typically obtain a 50% correct identification fraction with 4 mm square crystals [11].

There are three main effects that cause crystals other than the “target” crystal to be identified — imperfect collimation of the excitation beam, Compton scatter in the detector module, and electronic noise. Both imperfect collimation and detector Compton scatter lead to the adjacent 4 crystals being identified as the crystal of interaction more often than the other non-target crystals. Monte Carlo simulation suggests that Compton scatter alone results in each of the adjacent 4 crystals being identified 6% of the time [12], while imperfect collimation with a 3.1 mm fwhm beam alone results in each of the adjacent 4 crystals being illuminated 9% of the time. It is difficult to separate these two effects, but these predicted misidentification fractions in adjacent crystals are consistent with the measured fractions.

The value of the total energy threshold affects both the fraction of correctly identified events (as defined above), and the fraction of accepted events (defined as the fraction of those

0.8	0.3	0.7	0.2	0.2	0.3	0.5	0.0
0.5	0.4	0.4	0.3	0.2	0.5		
0.7	0.7	0.7	0.5	0.3	0.3		
2.0	5.8	2.4	0.9				
9.6	53	6.1	0.9				
3.4	5.6						
0.9	1.0						

1.1	0.7	9.0	58	8.9	0.9	0.6	0.0
0.6	0.5	2.0	5.9	1.8	0.7		
0.4	0.5	1.2	0.9	0.8	0.5		
0.3	0.7	0.5	0.5				
0.1	0.2	0.2	0.5				
1.4	0.1						
0.3	0.2						

62	14	1.3	0.6	0.2	0.3	0.4	0.0
7.7	2.7	1.1	0.3	0.1	0.4		
1.1	1.2	0.7	0.3	0.3	0.2		
0.4	0.5	0.4	0.3				
0.5	0.2	0.1	0.2				
1.2	0.2						
0.4	0.3						

Figure 5: The percentage of the time that each element is identified as the crystal of interaction for three “target” positions (identified by the thick border). Darkened regions indicate elements without amplifiers.

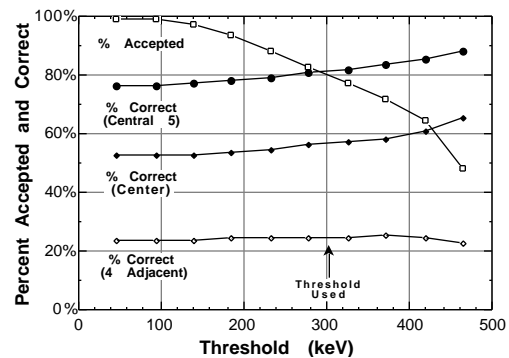


Figure 6: Percentage of events accepted and correctly identified in the LSO detector module as a function of total energy threshold, for a typical “target” element.

PMT triggers in which the total energy sum is above an energy threshold). Figure 6 plots the fraction of accepted events and correctly identified events as a function of the total energy threshold, using a PMT trigger threshold of 150 keV. The effects of imperfect beam collimation and Compton scatter can be somewhat reduced by redefining “correct” to be either the “target” crystal or one of the 4 adjacent crystals. With this definition, the crystal of interaction is properly identified $79 \pm 4\%$ of the time with a 300 keV total energy threshold, based on measurements of all 32 instrumented channels.

The timing resolution is determined by simultaneously exciting this detector module and a reference detector (plastic scintillator coupled to a fast photomultiplier tube) with annihilation photons and measuring the time difference between the reference detector and the photomultiplier tube discriminator output (with a 200 keV threshold). The timing distribution, shown in figure 7, has a width of 750 ps fwhm.

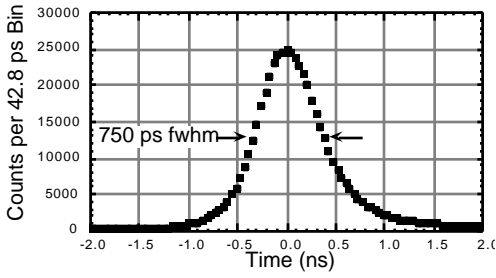


Figure 7: Coincidence timing resolution (with plastic scintillator) for the LSO detector module with a 200 keV threshold.

This width is dominated by the timing jitter of the detector module since the timing jitter of the reference detector is expected to be <300 ps. Thus, expected coincidence timing resolution of a pair of these detector modules is 1 ns fwhm — a factor of 3 better than is typically achieved with BGO.

B. Depth of Interaction

The detector module is rotated 90° relative to the electronically collimated beam of annihilation photons, allowing a 5.0 mm fwhm portion of the detector module to be excited at an arbitrary depth of interaction. Photodiode and total energy thresholds of 100 keV and 240 keV, respectively, are applied.

The detector module must be calibrated (on a crystal by crystal basis) in order to determine how the ratio between the photodiode and photomultiplier tube signals depends on interaction depth. Because of different quantum efficiencies, detector and amplifier gains, and ADC conversion factors, a given optical signal produces different measured signals in the photodetectors (64 photodiodes and 1 photomultiplier tube), or

$$\begin{aligned} PD_i(x) &= k_i L_{PD}(x) \\ PMT(x) &= k_{PMT} L_{PMT}(x). \end{aligned} \quad (1)$$

In equation (1), $L_{PD}(x)$ and $L_{PMT}(x)$ are the amount of light impinging on each photodetector when the crystal is excited by 511 keV photons at x mm depth, i is the crystal number, and the k 's are the efficiencies for converting light into output signal (in ADC counts) for each photodetector. In order to compare the measured photodetector outputs and compute a position estimator, it is necessary to measure the ratios $K_i = k_{PMT} / k_i$. To do this, we invoke a symmetry argument and assume that the light output from either 3x3 mm face of the LSO crystal depends only on the distance of the interaction from the crystal face, or

$$L_{PD}(x) = L_{PMT}(20-x). \quad (2)$$

We then obtain the gain normalization factor by dividing

$$K_i = \frac{PMT(18)}{PD_i(3)}, \quad (3)$$

where $PMT(18)$ is the centroid of the 511 keV photopeak in the photomultiplier tube when the detector is excited at a depth of 18 mm and $PD_i(3)$ is the 511 keV photopeak centroid in photodiode i when the detector is excited at a depth of 3 mm. The photodetector signals can then be converted into an equal energy scale and directly compared using these K_i . The positions 3 and 18 mm are chosen to represent the ends of the

crystal; when the excitation position is centered at the true ends (*i.e.* 0 and 20 mm), the event rate is too low due to the finite (5.0 mm fwhm) size of the collimated excitation beam.

The interaction position is measured on an event by event basis by computing a position estimator, defined as the fraction of the summed output from the photodetectors that is observed by the photodiode, or $=PD/(PD+PMT)$. Here PD is the largest pulse height (after normalization) observed in the photodiode array and PMT is the re-scaled pulse height observed by the photomultiplier tube. The beam is aimed from the left between the third and fourth rows (counting from the top as seen in figure 5). Figure 8 plots the estimator $PD/(PD+PMT)$ for all 10 photodiode channels in the third and fourth rows with the detector module excited at fixed positions of 3 and 18 mm depth.

The collimated excitation beam is scanned along the detector module, and at each depth of interaction the centroid and fwhm of the depth estimator $=PD/(PD+PMT)$ are computed. Figure 9 plots these measurements for the ten detector channels in rows 3 and 4 as a function of depth of interaction, with the fwhm of the depth estimator represented as error bars on the estimator. The centroid of the estimator is linearly dependent on depth, and the fwhm of this estimator is approximately depth independent.

Dividing the fwhm of the depth estimator by the slope yields the depth of interaction measurement resolution, which is 8 ± 1 mm fwhm for the ten excited channels. Our previous results [2] showed the DOI resolution to degrade with increasing depth since the uncertainty in this measurement was dominated by the photodiode signal to noise ratio. As the photodiode signal depends on depth and the noise is independent of depth, the signal to noise ratio (and thus DOI resolution) depended on depth. The present surface treatment significantly increases the light collection efficiency, nearly tripling the photodiode signal to noise ratio. As a result, position dependent variations in light collection efficiency (caused by the reflector coating) are now the dominant source of uncertainty in the estimator. We believe that further improvements in the surface treatment are possible, which will

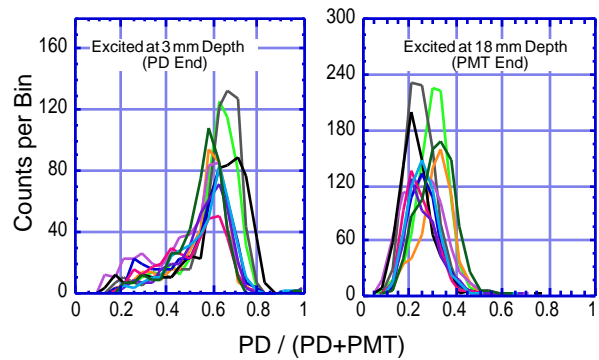


Figure 8: Distribution of the ratio $PD/(PD+PMT)$ with the detector module excited at fixed positions of 3 mm (left) and 18 mm (right). The ten “traces” in each peak correspond to the ten individual crystals in rows 3 and 4.

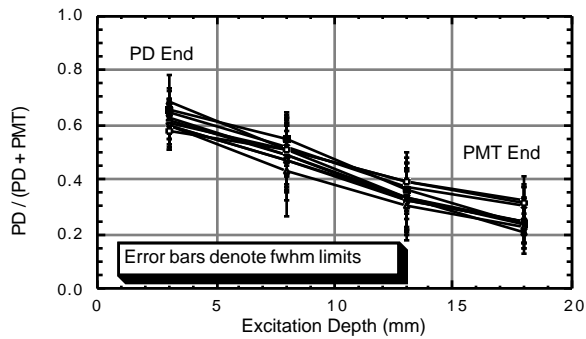


Figure 9: Value of the position estimator $PD/(PD+PMT)$ versus depth of interaction. The ten “traces” correspond to the ten individual crystals in rows 3 and 4. The width (fwhm) divided by the slope of the line gives the depth resolution.

reduce the uncertainty in the depth of interaction measurement and improve pulse height resolution.

The influence of the depth of interaction measurement resolution on the reconstructed point spread function has previously been reported [13]. Briefly summarized, Monte Carlo simulation predicts that a depth measurement resolution of 10 mm fwhm reduces the blurring due to radial elongation by a factor of two, while a depth measurement resolution of 5.0 mm fwhm effectively eliminates radial elongation. These results suggest that the measurement resolution achieved by the present detector module will substantially reduce the radial elongation artifact for this PET camera geometry.

IV. CONCLUSIONS

We have manufactured a 64 element prototype PET detector module (using LSO scintillator) in which the crystal of interaction is determined with a photodiode array. With 32 channels instrumented, the detector module identifies the “proper” crystal of interaction $79\pm 4\%$ of the time, where the definition of “proper” includes the “target” crystal and the 4 adjacent crystals. The timing and pulse height resolution for 511 keV photons are 750 ps fwhm and $24\pm 3\%$ fwhm respectively, yielding performance that exceeds conventional BGO based PET detector modules. In addition, the ratio of the signals observed by the photodiode and the photomultiplier tube is used to measure the depth of interaction on an event by event basis with an accuracy of 8 ± 1 mm fwhm. Hence, we feel that detector modules based on this design have tremendous potential in high performance, yet practical, PET cameras.

V. ACKNOWLEDGMENTS

We would like to thank Mr. Yamamoto of Hamamatsu Photonics for many interesting discussions, culminating with the photodiode array used herein. This work was supported in part by the Director, Office of Energy Research, Office of Health and Environmental Research, Medical Applications and Biophysical Research Division of the U.S. Department of Energy under contract No. DE-AC03-76SF00098, in part by the National Institutes of Health, National Heart, Lung, and Blood Institute, National Cancer Institute, and National

Institute of Neurological Disorders and Stroke under grants No. P01-HL25840, No. R01-CA67911, and No. R01-NS29655, and in part by the Breast Cancer Fund of the State of California through the Breast Cancer Research Program of the University of California under grant No. 1RB-0068. Reference to a company or product name does not imply approval or recommendation by the University of California or the U.S. Department of Energy to the exclusion of others that may be suitable.

VI. REFERENCES

- [1] W. W. Moses, S. E. Derenzo, R. Nutt, et al., “Performance of a PET detector module utilizing an array of silicon photodiodes to identify the crystal of interaction,” *IEEE Trans. Nucl. Sci.*, vol. NS-40, pp. 1036–1040, 1993.
- [2] W. W. Moses, S. E. Derenzo, C. L. Melcher, et al., “A room temperature LSO / PIN photodiode PET detector module that measures depth of interaction,” *IEEE Trans. Nucl. Sci.*, vol. NS-42, pp. 1085–1089, 1995.
- [3] J. G. Rogers, C. Moisan, E. M. Hoskinson, et al., “A practical block detector for a depth-encoding PET camera,” *IEEE Trans. Nucl. Sci.*, vol. NS-43, pp. 3240–3248, 1996.
- [4] C. Carrier, C. Martel, D. Schmitt, et al., “Design of a high resolution Positron Emission Tomograph using solid state scintillation detectors,” *IEEE Trans. Nucl. Sci.*, vol. NS-35, pp. 685–690, 1988.
- [5] P. Bartzakos and C. J. Thompson, “A depth-encoded PET detector,” *IEEE Trans. Nucl. Sci.*, vol. NS-38, pp. 732–738, 1991.
- [6] M. E. Casey, L. Eriksson, M. Schmand, et al., “Investigation of LSO crystals for high spatial resolution positron emission tomography,” *IEEE Trans. Nucl. Sci.*, vol. NS-44, (submitted for publication), 1997.
- [7] W. Worstell, O. Johnson, and V. Zawarzin, “Development of a high-resolution PET detector using LSO and wavelength-shifting fibers,” Proceedings of The 1995 IEEE Nuclear Science Symposium and Medical Imaging Conference, pp. 1756–1760, San Francisco.
- [8] C. L. Melcher and J. S. Schweitzer, “Cerium-doped lutetium oxyorthosilicate: a fast, efficient new scintillator,” *IEEE Trans. Nucl. Sci.*, vol. NS-39, pp. 502–505, 1992.
- [9] W. W. Moses, I. Kipnis, and M. H. Ho, “A 16-channel charge sensitive amplifier IC for a PIN photodiode array based PET detector module,” *IEEE Trans. Nucl. Sci.*, vol. NS-41, pp. 1469–1472, 1994.
- [10] W. W. Moses, E. Beuville, and M. H. Ho, “A “winner-take-all” IC for determining the crystal of interaction in PET detectors,” *IEEE Trans. Nucl. Sci.*, vol. NS-43, pp. 1615–1618, 1996.
- [11] S. R. Cherry, M. P. Tornai, C. S. Levin, et al., “A comparison of PET detector modules employing rectangular and round photomultiplier tubes,” *IEEE Trans. Nucl. Sci.*, vol. NS-42, pp. 1064–1068, 1995.
- [12] K. A. Comanor and W. W. Moses, “Algorithms to identify detector Compton scatter in PET modules,” *IEEE Trans. Nucl. Sci.*, vol. NS-43, pp. 2213–2218, 1996.
- [13] W. W. Moses, R. H. Huesman, and S. E. Derenzo, “A new algorithm for using depth-of-interaction measurement information in PET data acquisition,” *J. Nucl. Med.*, vol. NS-32, pp. 995, 1991.